Cation intermixing and electronic deviations at the insulating $LaCrO_3/SrTiO_3(001)$ interface

R. Colby,[1] L. Qiao,[2] K. H. L. Zhang,[2] V. Shutthanandan,[1] J. Ciston,[3] B. Kabius,[1] and S. A. Chambers[2]
[1]*Environmental Molecular Sciences Laboratory, Pacific Northwest National Laboratory, Richland, Washington 99352, USA*
[2]*Fundamental and Computational Sciences Directorate, Pacific Northwest National Laboratory, Richland, Washington 99352, USA*
[3]*National Center for Electron Microscopy, Lawrence Berkeley National Laboratory, Berkeley, California 94720, USA*
(Received 9 May 2013; revised manuscript received 10 July 2013; published 29 October 2013)

The interface between polar perovskite $LaCrO_3$ and nonpolar $SrTiO_3(001)$ grown by molecular beam epitaxy is examined using a combination of electron microscopy, spectroscopy, and Rutherford backscattering spectrometry. The *A*-site cations of these ABO_3 perovskites are found to diffuse across the interface to a greater extent than the *B*-site cations, based on high-angle annular dark-field scanning transmission electron microscopy, energy-dispersive x-ray spectroscopy, and electron-energy-loss spectroscopy (EELS). The *B*-site cation valences are shown to be partially reduced near the interface by analysis of EELS near-edge structures. The location and direction of these electronic modifications do not intuitively compensate the charge imbalance imposed by uneven cation interdiffusion, and yet both the film and interface are insulating. These results highlight the importance of considering both the physical and electronic structure of such complex interfaces in determining their characteristics.

DOI: 10.1103/PhysRevB.88.155325 PACS number(s): 73.20.Hb, 68.37.Ma

I. INTRODUCTION

Complex oxide interfaces and the compelling electronic and magnetic phenomena they exhibit are topics of considerable current interest. The $LaAlO_3/SrTiO_3(001)$ interface (L*A*O/STO) has received the most attention in recent years, following the observation of an anomalous conductivity at the interface between the nonpolar STO and the polar $LaAlO_3$, both of which are insulating in the bulk.[1–6] Following this discovery, a variety of polar and nonpolar transition metal perovskite oxides on nonpolar STO have been considered, including $SrMnO_3$/STO,[7–9] $LaMnO_3$/STO,[10,11] $GdTiO_3$/STO,[12] $LaGaO_3$/STO,[13] $LaVO_3$/STO and $LaTiO_3$/STO,[14,15] $DyScO_3$/STO,[16] $KTaO_3$/STO,[17] and $LaCrO_3$/STO.[18] The observation of interfacial conductivity in these systems has been inconsistent, and the mechanism or mechanisms governing the conductivity remains unresolved. For a polar ABO_3 perovskite with A^{3+} and B^{3+} cations, alternating (001) AO/BO_2 layers carry a charge of $-1\,e^-/+1\,e^-$ per layer, per square unit cell (u.c.), leading to a residual $\pm 1e^-$/u.c.[2] discontinuity at the interface to a nonpolar perovskite such as STO(001). The original explanation hinges upon alleviation of the polar discontinuity by an electronic reconstruction of the terminal STO layer.[19–21] For instance, the similar *n*-type conductivity observed for $LaVO_3$/STO, $LaAlO_3$/STO, and $LaGaO_3$/STO has been attributed to a partial change of the terminal $TiO_2(001)$ layer's Ti valence state from Ti^{4+} towards $Ti^{3.5+}$, for which there has been some evidence.[21–23] However, the $LaMnO_3$/STO interface, which should also be *n* type, has been found to be insulating[13] and the $KTaO_3$/STO interface, which should be *p* type, was found to be *n* type.[17] The issue has been further complicated by a growing body of data indicating that many such polar/nonpolar perovskite oxide interfaces are not atomically abrupt, often exhibiting cation mixing over several unit cells.[4,24] Inequivalent extents of diffusion of *A*- and *B*-site cations have been observed in some cases[25] and could also readily explain the net doping of the interface, but may not resolve the polar discontinuity. Furthermore, direct evidence for a built-in potential within the polar film sufficiently large to match an electronic reconstruction of only the terminal STO layer has not yet been demonstrated.[4,26,27] Evidence suggests that a combination of electronic and structural effects govern the various properties of these polar/nonpolar perovskite interfaces.

To gain further insight, we investigate in detail a system that specifically does not exhibit interfacial conductivity—$LaCrO_3$ (LCO) on STO(001). The choice of a transition metal *B*-site cation, such as Cr, introduces low-lying *d* orbitals on the *B* site of the polar perovskite. Thus, Cr could act as either an acceptor or a donor in LCO by adopting a Cr^{2+} or Cr^{4+} state. Previous work, based upon high-energy-resolution x-ray photoelectron core-level spectroscopy as a function of LCO film thickness in conjunction with first-principles theory, has suggested that the absence of conductivity may result from charge reorganization within the LCO layer, as opposed to the net transfer of charge from LCO to STO.[18] This charge reorganization was predicted to be facilitated by low-lying *d* orbitals on Cr sites as well as the presence of outdiffused Ti at *B* sites in the LCO, for which preliminary evidence was presented.[18] In this study, the atomic concentration profiles and local electronic structure are investigated across LCO/STO(001) interfaces for films of various thickness, based upon a combination of scanning transmission electron microscopy (STEM), energy-dispersive x-ray spectroscopy (EDS), electron-energy-loss spectroscopy (EELS), energy-filtered transmission electron microscopy (EFTEM), and conventional and high-resolution Rutherford backscattering spectrometry (RBS and HRRBS).

II. EXPERIMENTAL METHODS

Structurally excellent LCO epitaxial films were grown on STO(001) by molecular beam epitaxy (MBE).[28] The pseudocubic phase of LCO has an in-plane lattice mismatch of only −0.5%, and x-ray diffraction has revealed that films of up to 500-Å thickness are coherently strained to the substrate. There is no measurable conductivity at the interface.[18]

MBE allows for more precise control over layer deposition, more reproducible composition control, and less point defect creation due to the lower incoming particle energies than some of the alternative approaches common for growth of perovskite thin films, such as pulsed laser deposition (PLD).[3] The conditions used result in layer-by-layer growth, thereby preserving the terrace-step structure of the TiO_2-terminated STO(001) substrate. Cross sections were prepared with a nominal [100] surface normal using an FEI Helios dual-beam focused ion beam/scanning electron microscope (FIB/SEM) equipped with an Omniprobe, using the lift-out technique.[29] The extracted sections were further thinned at lower energies ($\geqslant$500 eV) with Ar^+ ions, with a sample stage cooled by liquid nitrogen, using a Fischione 1040 NanoMill. Images of the interface were recorded using high-angle annular dark-field scanning transmission electron microscopy (HAADF-STEM) with a probe-corrected FEI Titan microscope at a 300-kV acceleration voltage. HAADF-STEM images are dominated by atomic number based contrast, allowing differentiation between the *A*- and *B*-site atomic columns, as well as discriminating La-rich from Sr-rich *A*-site atomic columns, when viewed along the [100] direction (see Fig. 1). Cross sections were prepared for LCO film thicknesses ranging from 5 to 125 u.c. Data were collected for various cross-section thicknesses from $\sim$100 to $<$20 nm, and all included images were acquired with annular detector inner angles greater than $\sim$60 mrad, found to result in minimal strain contrast. EDS and EELS were collected in STEM mode at 300 kV with, respectively, a 0.13 sr EDAX detector, and a Gatan QuantumER imaging filter (GIF). EELS energy resolution was typically between 0.7 and 0.9 eV. STEM-EDS profiles were collected with the sample tilted to the [120] zone axis to minimize detector shadowing while maintaining an edge-on view of the interface to avoid artificial broadening. Portions of the EELS analysis employed the Cornell Spectrum Imager ImageJ plugin.[30] EFTEM images were acquired on the spherical (C_s) and chromatic aberration (C_c) corrected TEAM I microscope at 80 kV.

RBS was performed with He^+ ions accelerated to 400 keV, with a current of 5 nA. The depth resolution of conventional RBS is limited by the energy resolution of the Si surface barrier detectors used in current instrumentation ($\sim$15 keV). To improve the depth sensitivity, a high-energy-resolution (1–2 keV) magnetic sector detector coupled with a microchannel plate was used. The HRRBS detector was positioned such that the backscattered He ions entered the detector at a scattering angle of 105°. Channeling data were obtained with the incident beam aligned along [001] ($\theta = 0°$) and nonaligned, or random, spectra were obtained at various incident angles θ ranging from 7° to 31°. The total dose was limited to 150 μC in order to minimize beam damage. At this beam energy the stopping power is maximized, also improving depth resolution. Rocking curves were measured using conventional RBS in order to determine out-of-plane lattice parameters for the LCO films. Atom profiles normal to the interface were determined by fitting the random spectra to predictions generated using SIMNRA (Ref. 31) computer code. For these simulations, the probed volume was manually divided into several thin layers, each with a separate thickness and composition. Experimental parameters such as incident ion atomic number and energy, incident and backscattered angles, detector energy calibration values and solid angle, and total incident charge are considered in the calculations. The composition profiles and film areal densities are then systematically varied until the best fit to the experimental data is obtained. The resulting models represent consistent, but not necessarily unique solutions for the atomic concentration profiles.

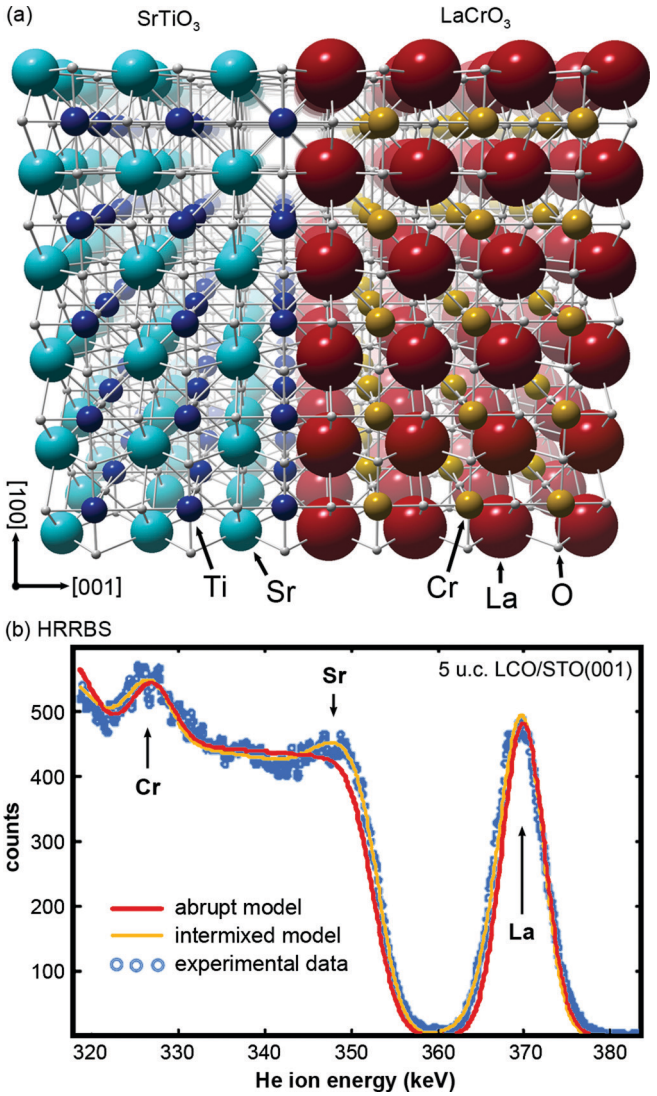

FIG. 1. (Color online) (a) Schematic model of an ideal abrupt $LaCrO_3/SrTiO_3(001)$ interface, viewed along the [010] direction. The atom radii are scaled by Z number, to help highlight comparison to the Z-based contrast of HAADF-STEM and RBS. (b) Random HRRBS spectrum for a 5-u.c.-thick LCO/STO(001) film (blue circles), along with SIMNRA simulations for the abrupt and optimized intermixed interfaces (red and orange lines, respectively). It is clear that an intermixed model fits more accurately, particularly for the Sr ($\sim$350 keV) and La ($\sim$370 keV) signals.

III. RESULTS

RBS is more sensitive to heavier elements due to cross sections that scale as Z^2. For LCO/STO, the sensitivity thus decreases in the order La > Sr > Cr > Ti > O. The data for a 5-u.c.-thick LCO film are shown with the abrupt

and optimized intermixed SIMNRA calculations [Fig. 1(b)]. Modeling an abrupt interface, drawn as a red curve in Fig. 1(b), results in clear deviations from experimental measurements on the low-energy side of the La peak, as well as along the leading edge of the Sr plateau. However, modeling an optimized intermixed interface (orange curve) produces better agreement. Based upon this intermixed model, only the final 2 u.c. of LCO have their full complement of La (20 at. %). The La atomic concentration profile has a width at 10%–90% intensity of ∼6 u.c., but the La concentration does not reach zero until a depth of ∼10 u.c. Cr sensitivity is considerably lower, but including a Cr diffusion approximately matching that of La marginally improves the quality of the fit.

With aberration-corrected STEM, the *A*-site (Sr, La) and the *B*-site (Ti, Cr) atomic columns are very clearly distinguished when viewing along the [100] direction. The intensity measured by HAADF-STEM predominantly increases with increasing atomic number, such that the Sr:La and Ti:Cr atom ratios can be assessed using the intensity of successive columns normal to the interface. The *A*-site atomic columns provide a clearer measure of the local cation ratio, as the heavier La and Sr scatter more strongly than the lighter *B*-site atoms (higher signal to noise), and the atomic number difference between La and Sr (19) is larger than for Cr and Ti (2). The *B*-site columns also consist of alternating cations and oxygen anions in the [100] projection. Nevertheless, all films examined with HAADF-STEM show a gradual change in atomic-column intensity along both the *A* and *B* sites across the interface, which can be interpreted here as evidence of cation intermixing. In a 130-u.c.-thick LCO film, for instance, the *A*-site intensity changes over a distance of 4–7 u.c. (depending upon the manner of background interpretation). A representative image from a ∼40-nm cross section is presented in Fig. 2(a). Intensities were measured along the [001] direction integrated over a ∼0.8-Å-wide line, traversing either the *A*-site or *B*-site columns, as demonstrated in Fig. 2(b).

A variety of approaches has been utilized previously for determining the width of an interface using HAADF-STEM data. These include the use of best-fit curves and multiply smoothed profiles, along with various methods of background subtraction and atomic-column peak fitting. Curve fitting and similar options neglect the contribution of beam broadening to the background between strongly channeling atomic columns, and can overestimate the interface width. The background subtraction schemes do not account for potential variations in oxygen concentration or crystal structure, and can underestimate of the extent of interdiffusion. The width between 10% and 90% of the intensity of best-fit curves thus results in the largest assessment of the extent of intermixing, and amounts to 7 u.c. for the 130-u.c.-thick sample (rounded to the nearest unit cell). A simple background subtraction scheme calculated using the linear interpolation of adjacent atomic-column minima results in the most abrupt assessment of the interface, yielding a width of nearly 4 u.c. for the 130-u.c.-thick film. These two approaches thus provide reasonable upper and lower limits for the interface width at this total film thickness. From here on, the best-fit 10%–90% widths will be reported with an understanding that they yield an upper limit. By either technique, the interface width exceeds the probe size or

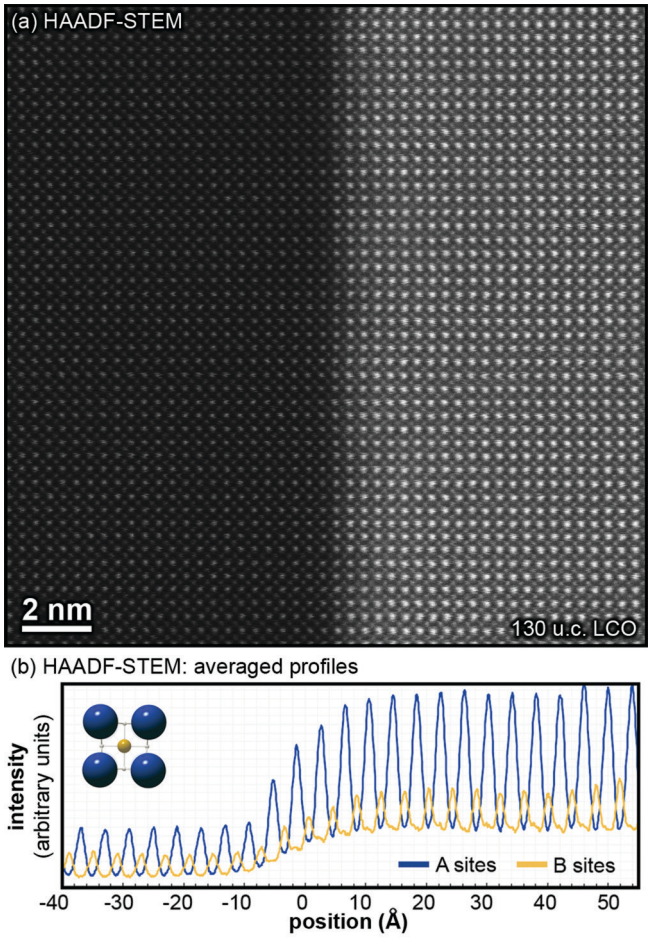

FIG. 2. (Color online) (a) In a representative cross-sectional HAADF-STEM image of a typical 130-u.c.-thick LCO/STO sample, there is clearly a gradual change in column intensity across the interface, indicating that the LCO/STO interface is not abrupt (image is adjusted for systematic sample drift during data acquisition, but otherwise unprocessed). (b) To more quantitatively analyze the extent of interdiffusion at the interface, the HAADF intensity has been integrated (from the original, unprocessed data) and averaged over 30, 0.8-Å-wide lines situated separately along the *A*-site (dark blue) and *B*-site columns (light orange).

beam broadening within the sample and, thus, cation mixing is clearly occurring. The *A*- and *B*-site profiles are also asymmetric with respect to the interface, being sharper on the STO side. This observation is made for other LCO film thicknesses as well. This result may mean that the extent of La and Cr lost from the LCO side of the interface is greater than the loss of Sr and Ti from the substrate.

To assess individual atomic concentration profiles, EDS, EELS, and EFTEM were performed for a 25-u.c.-thick LCO film. This thickness is large enough to include a uniform stoichiometric region of LCO away from the interface as a built-in reference and thin enough to perform complementary HRRBS measurements. STEM-EDS profiles can be independently measured for Sr, Ti, and La. The Cr K_α peak overlaps with the comparatively weak La L_β peak, and is thus only approximate [Fig. 3(a)]. The extents of Cr and Ti diffusion differ by less than half a unit cell, both being 7(1) u.c.

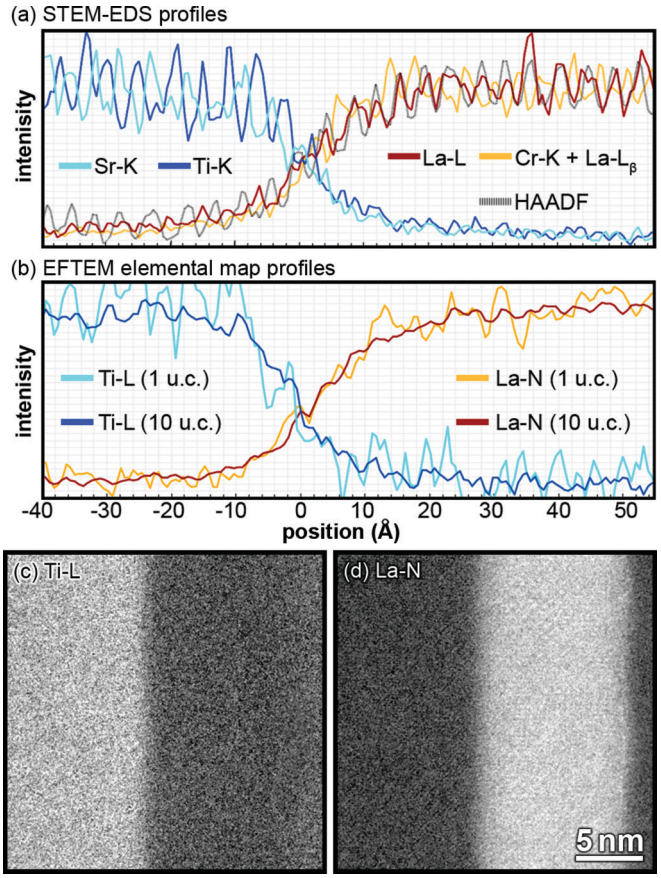

FIG. 3. (Color online) Comparison of individual atomic concentration profiles for a 25-u.c.-thick LCO film. (a) EDS line profiles extracted from the raw, integrated peak areas, and compared with concurrently collected HAADF intensity (gray line) to account for sample drift. The combined Cr-K and La-L_β signal should be predominantly indicative of Cr (in agreement with the adjoining La and HAADF profiles). (b) Line profiles extracted from chromatic-aberration-corrected EFTEM elemental maps (c), (d), for the Ti L and La N edges. Profiles acquired with linewidths of roughly 1 and 10 u.c. are included for each. Interfacial inhomogeneities are arguably visible in both maps. For both EDS and EFTEM profiles, the intensities were independently normalized to facilitate comparison, and the vertical axes are in arbitrary units.

when rounded to the nearest unit cell. The extents of La and Sr diffusion are greater, 9(1) u.c. and 11(1) u.c., respectively, when rounded to the nearest unit cell. Similar measurements at different locations along the interface consistently reveal a greater extent of mixing of the A-site cations than the B-site cations, and longer diffusion lengths for La than for Sr.

EFTEM imaging allows for parallel collection of spectral information over a larger, two-dimensional area, and enables assessment of local variations in cation mixing. With chromatic aberration correction, inelastically scattered electrons at various energy losses share a common focus, and elemental mapping of features down to 4 Å in size has been demonstrated.[32] Filtered images were acquired for at least two energies below the relevant La and Ti core-loss edges, and at least one energy beyond that edge (10 eV windows used for the La N edge, and 23 eV for the Ti K edge). The element-specific signal was extracted using a slope exponent measured using at least two preedge windows.[33] Maps obtained for the La N and Ti L edges [Figs. 3(c) and 3(d)] are in good agreement with EDS results. EFTEM intensity profiles have been extracted for comparison, similarly self-normalized, for 1- and 10-u.c. linewidths and are seen in Fig. 3(b). The 10%–90% widths of the best-fit curves for the 10-u.c.-wide profiles are 6 u.c. for the Ti, and 9 u.c. for La, to the nearest unit cell. The greater extent of diffusion for the A-site cations compared to the B-site cations is in agreement with the EDS results. The broader interface measured by EDS as compared to EFTEM is expected, due to the minor emission of x rays by secondary processes from a volume larger than that excited directly by the electron beam.[33] With these two-dimensional maps, one can see local inhomogeneities along the interface for both the Ti and La. However, the local extent of interdiffusion remains greater for La than Ti.

The spectroscopic results discussed above indicate an inequivalent extent of A- and B-site cation diffusion. A La^{3+} cation on a Sr^{2+} site in STO is a well-studied, electrically active donor,[34] whereas a Cr^{3+} cation on a Ti^{4+} site is expected to be deep-level acceptor. An imbalance might thus be expected to lead to conductivity. To better understand and visualize the effect of cation mixing as an isolated effect, we consider a simple model. Assuming standard formal charges from bulk LCO and STO (Ti^{4+}, Sr^{2+}, Cr^{3+}, and La^{3+}) and perfect oxygen stoichiometry on both sides of the interface, the net electronic charge per unit cell along the interface can be calculated from the atomic concentration profiles, and these are shown in Fig. 4(a). The results suggest that, in the absence of any electronic modifications, there would be an n-type excess on the STO side of the interface and a larger p-type excess on the LCO side. The integrated charge across the interface—the sum of the gray and black portions of the plot in Fig. 4(a)—would be 0.2 e/u.c. or $\sim 10^{14}$ e/cm^2 (p type), which is more than sufficient to give rise to a conducting layer. Inasmuch as these interfaces are insulating, cation mixing must not be the only effect at play here.

This model provides a useful consistency check for the measurements of the cation concentration profiles. An abrupt, unreconstructed LCO/STO interface has a 1 e/u.c. polarization, or dipole. Monotonic diffusion of the cations across the entire interface would not change the net polarization, unless cations from the substrate diffuse all the way to the film surface. The net polarization—the difference between the gray and black portions of Fig. 4(a)—would be ~ 0.9 e^-/u.c., in quite reasonable agreement.

The above exercise seems to suggest that some degree of electronic modification of cation valence states near the interface must occur to result in a nonconducting interface. The net cationic charge imbalance could also be relieved by a partial Cr^{4+} B-site occupation on the LCO side of the interface, or either Cr^{2+} or Ti^{3+} on the STO side. Cr^{2+} is uncommon in oxides and the rare instances observed at room temperatures and pressures (e.g., phyllosilicate $CaCrSi_4O_{10}$, or Cr-bearing lunar basalts[35]) are not octahedrally coordinated. The Ti in $LaTiO_3$/STO(001) films should exhibit a +3 charge.[36] Valence states of Ti and Cr can be locally interrogated using EELS via near-edge structure changes (ELNES). For the 25-u.c. LCO/STO interface, the valence state of the Cr can be estimated from the L_3:L_2 ratio.[37] Peak fitting with a

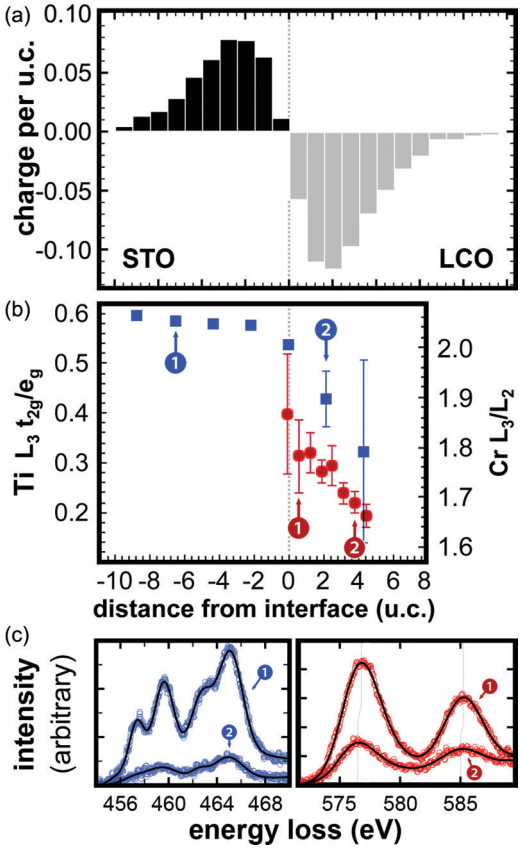

FIG. 4. (Color online) (a) Calculation of the charge per unit cell across the interface assuming no change in cation valency (i.e., a net charge equal to 3[La] + 2[Sr] + 3[Cr] + 4[Ti]–6) using atomic concentrations derived from EDS data. This demonstrates that in the absence of local electronic modifications, there would be a net excess of $\sim 0.2\ e^-$/u.c. on the LCO side of the interface (or $10^{14}\ e/\mathrm{cm}^2$). (b) However, measurement of the Ti L (blue squares) and Cr L edges (red circles) with EELS indicates that there is some degree of valence change for the B-site cations. A partial shift in the Ti valence, from Ti^{4+} towards Ti^{3+} going into the LCO, is demonstrated by fitting L-edge t_{2g}:e_g ratios (blue squares). The Ti L_3 ratios are shown, as the L_3 splitting should be more pronounced, but the L_2 edge trend is the same. There is also a partial change in the Cr oxidation state approaching the interface from Cr^{3+} to Cr^{2+}, evidenced by increasing L_3:L_2 ratios. There is also a minor chemical shift (~ -0.2 eV) as expected from a partial shift towards Cr^{2+}. Error bars are based upon the fitting error, which increases for decreasing concentrations of Ti or Cr. (c) Representative Ti L- and Cr L-edge spectra (1) away from the interface and (2) near the interface on the LCO side are included for the points indicated in (b), with the raw data indicated by hollow circles (blue or red) and the result of peak fitting traced in black.

polynomial background from 568 to 600 eV reproduces the L_3:L_2 ratios for Cr^{3+} reported using approaches described elsewhere,[37] without iterative modeling of the postedge background or manual integration window selection (the approach of Pearson *et al.*[38] was also tested for these data sets, and produces consistent results). While there is no EELS literature on Cr^{2+}-containing oxides, other Cr^{2+}-containing compounds have higher L_3:L_2 ratios than Cr^{3+} (Cr^{4+}-containing oxides exhibit L_3:L_2 ratios that are lower than those for Cr^{3+}).[37] The Cr L_3:L_2 ratio increases as the interface is approached, and a chemical shift of up to -0.3 eV also occurs, consistent with partial B-site occupancy with Cr^{2+} [Figs. 4(b) and 4(c)]. Within the STO where the Cr concentration is less, L-edge fitting error is too large to be useful, hindered by differences in the bulk LCO and STO O K-edge structures (the O K-edge extended structure encroaches upon the Cr L edge). Similarly fitting the Ti $L_{3,2}$ t_{2g} and e_g features with Gaussian peaks reveals a small but reproducible and statistically significant decrease in the t_{2g}:e_g ratios near the interface, mostly on the LCO side, as seen in Figs. 4(b) and 4(c). Such behavior is commonly attributed to the formation of a partial Ti^{3+} valence.[22,23] The La L edge does not reveal any local changes in L_3:L_2 ratio or peak position, confirming La^{3+} across the interface, as expected. It was not possible to measure Sr in this manner, but states other than Sr^{2+} would not be expected.

As spectroscopic evidence suggests nominally well-behaved, monotonically changing concentration profiles for each cation, the average extents of interdiffusion can be estimated using HAADF-STEM contrast. To this end, HAADF-STEM analysis was compared for films of 5-, 15-, 25-, and 130-u.c. LCO thicknesses (Fig. 5). There is a general trend of an increased extent of cation mixing with increased film thickness [Fig. 5(b)]. This trend could be explained by kinetically limited cation diffusion lengths at the growth temperature.

For the samples discussed above, there was typically a difference of approximately half a unit cell between the extent of interdiffusion of the A and B sites at any location or thickness. As mentioned above, spectroscopic measurements indicate a distinctly more abrupt interface for B-site cations relative to the A-site cations. This suggests that despite the appearance of well-separated atomic columns in HAADF-STEM measurement—the probe is <1 Å and the A- and B-site columns are separated by >1.9 Å in [100] projection—contrast at the B-site columns is partially convoluted with the intensity from neighboring A-site columns. Recalling that the difference in the average atomic number for Cr:O and Ti:O columns (1) is very small relative to that for La and Sr (19), this effect should not have a significant impact on the measurement of the A-site diffusion lengths, or any of the conclusions in this study. Additionally, nominally flat STO(001) substrates do have regular step edges, typically 1 u.c. in height. Previous atomic force microscopy (AFM) measurements indicate roughly [001]-oriented steps spaced $\sim$40–200 nm apart, depending on the miscut. FIB-prepared samples are typically extracted to within $\sim 10^\circ$ of a [001] direction, but never precisely along the plane. It is exceptionally unlikely for multiple 40–50-nm-thick cross sections to include a step edge perpendicular to the viewing direction across a significant portion of the cross-section interface (typically $>10\ \mu$m), but it could theoretically add 1 u.c. to measurements of the interface widths. There are indications in several of the STO(001) supported films that the step edges are parallel to the view direction, such that local measurements would be insensitive to their presence. Nevertheless, the error bars on the measurement of the extent of interdiffusion have been set at a minimum of 1 u.c. to account for this possibility.

The extent of intermixing for films of various thicknesses of LCO was also measured by HRRBS. As the Cr, Ti, and O features sit atop the Sr plateau and have a lower sensitivity,

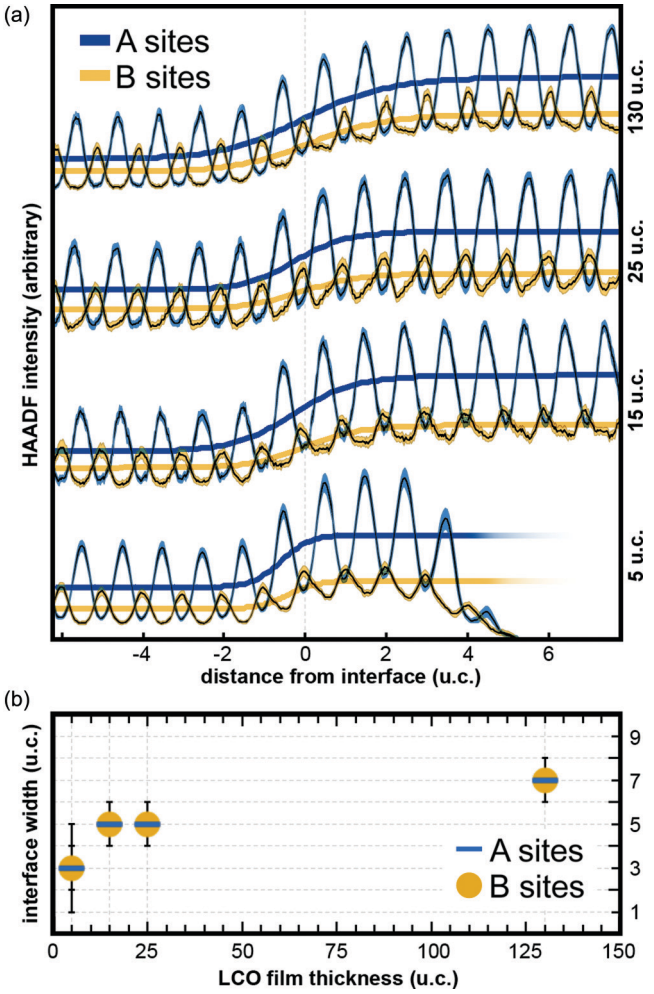

FIG. 5. (Color online) (a) Averaged profiles for 5-, 15-, 25-, and 130-u.c.-thick LCO films on STO, as measured by HAADF-STEM intensity (shifted vertically for comparison). Each region included in this examination was ~40–50 nm thick in cross section. One standard deviation of the measurement at each position is included as a colored range around the measured profiles. The position is labeled in unit cells based upon the spacing of STO, and the zero position of the interface is not quantitative here. The widths at 10%–90% intensity of the best-fit curves for several such measurements are summarized in (b), rounded to the nearest unit cell. The 2 u.c. error bars on the 5 u.c. data point correspond to the *B*-site measurement. The data suggest an increasing extent of interdiffusion with increasing LCO film thickness

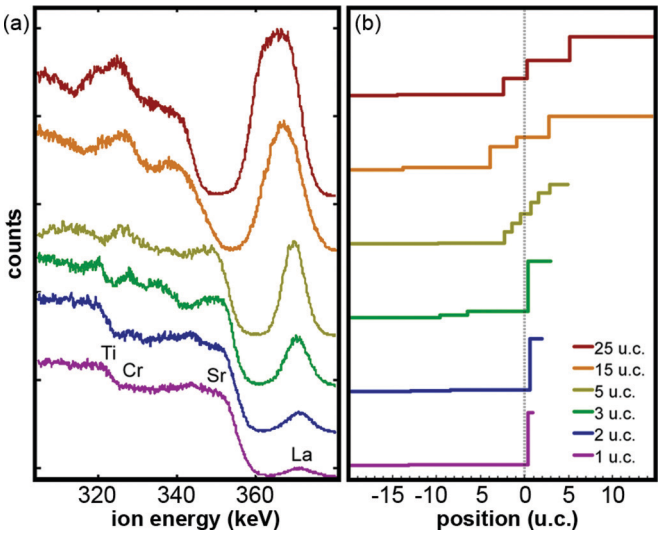

FIG. 6. (Color online) (a) Random HRRBS spectra for LCO/STO films of various thicknesses, and (b) the La atom profiles resulting from fitting these spectra with SIMNRA calculations. The original interface position was estimated by multiplying the areal density from the simulations by the atom number density in coherently strained LCO and shifting this scale by the actual film thickness from RHEED intensity oscillations. The abrupt steps are an artifact of the models, and do not imply discrete concentration shifts.

the La peak is the most reliable for film-to-film comparison. La depth profiles were extracted for LCO films of various thicknesses, as seen in Fig. 6. For LCO thicknesses in excess of 5 u.c., a clearly discernible region of graded composition forms near the interface. The graded region straddling the original interface position has a width of ~2 nm (~5 u.c.) for film thicknesses of 5–25 u.c., in qualitative agreement with STEM, EDS, and EELS results. The steplike nature of these models should not be overinterpreted and does not, for instance, imply atomically sharp concentration changes. In all cases, low levels (a few to less than 1 at. %) of La are detected to depths well beyond the original interface, sometimes tens of unit cells deep into the STO. Such long, low-concentration tails are unlikely to be detectable by HAADF-STEM, EELS, or EDS. This result further emphasizes that cation interdiffusion must be considered in such systems, and that the unequal extents of cation diffusion alone do not guarantee conductivity.

IV. DISCUSSION

Thus far, it has been demonstrated that the LCO/STO interface is not abrupt, the *A*- and *B*-site cations diffuse across the interface to different extents, and the charge states of both *B*-site cations are modified on the LCO side of the interface. The imbalanced diffusion alone would result in a net *p*-type region on the LCO side of the interface. A local increase in the Cr valence (Cr^{3-4+}) could have accounted for this imbalance, but ELNES measurements instead suggest a local reduction (Cr^{2-3+}). The structure of the Ti *L* edge also suggests local reduction from Ti^{4+} to (Ti^{3-4+}) on the LCO side of the interface. At first glance these results are at odds with an insulating interface. However, there are several means by which one could readily imagine balancing the net charge near the interface. Oxygen vacancies in the near-interface region of the LCO would be the simplest possibility. The local oxygen content has been measured using EELS—by integration of the background-subtracted signal under the O *K* edge, after deconvolution by the simultaneously acquired low-loss signal to account for local differences in the scattering cross section[33]—and no discernible deficiency of oxygen in the near-interface region is found. However, these measurements have a standard deviation of ~6% of the atomic oxygen content. Based upon the cation concentrations measured by EDS and the calculations shown in Fig. 4(a), the net charge imbalance could be compensated by an average oxygen deficiency of only 0.4 at. % per u.c. over the first

7 u.c. of the LCO (while decreasing the net polarization) or instead in the first 7 u.c. of the STO (while increasing the net polarization). These values are below expected measurable limits: Each u.c. imaged in projection through the typical cross-sectional TEM samples used here is ∼100 u.c. deep, and would contain less than two missing oxygen atoms. At these minuscule concentrations the effects of free surfaces and sample preparation artifacts would prevent defensible quantification of the oxygen vacancies by EELS at these interfaces, even if the detection sensitivity were sufficient.

The Cr oxidation state reduction near the interface may also suggest a local oxygen deficiency. The interdiffusion of all four cations and the possibility of oxygen vacancies hinder accurate quantification of local charge states from ELNES line shapes. Estimating the valence states of the Ti and Cr by fitting to reference data (e.g., Refs. 21 and 37) suggests the Ti goes from ∼4+ to ∼3+ within 4 u.c. after the interface, and that the Cr reduces to ∼2.1+ at the interface, but the statistical uncertainty is too large to improve the previously mentioned estimates of the necessary oxygen deficiency (see Supplemental Material,[39] Fig. S1). The near-edge structure of the O K edge changes gradually across the interface from that of bulk STO to that of bulk LCO, with no features indicating oxygen vacancies.

The presence of Ti^{3+} in the LCO is arguably unsurprising: B-site Ti in $LaTiO_3$ should have a 3+ oxidation state. Octahedrally coordinated Cr^{2+} is more unusual. The argument could be made that Cr reduces to partial Cr^{2+} near the interface to compensate the residual Ti^{4+} that has diffused into the LCO, as the Cr and Ti trend oppositely with position. This alone is insufficient to explain why the interface is not conducting. Another possibility is the presence of Cr antisite defects, with Cr^{2+} residing on A sites. Previous work has suggested the formation of stable antisite defects in LCO to accommodate changes in the La:Cr ratio, with calculations suggesting Cr_{La} antisites should form in Cr-rich LCO films.[40] The imbalanced cation interdiffusion profiles measured here would suggest a locally Cr-rich region near the interface correlating with where the Cr^{2-3+} is found. Antisites in the LCO that are effectively Cr_{Sr}-like—e.g., a case where an antisite has more in-diffused Ti B-site neighbors than Cr—would provide a motivation for Cr^{2-3+} (Cr_{La} should still be 3+). As an additional benefit, the presence of Cr_{Sr}-like antisite defects in the LCO could explain the different extents of La and Sr interdiffusion. Assuming that interdiffusion occurred by switching cations across the interface, the La/Sr imbalance would have otherwise required, for instance, Sr-site vacancies in the STO (which remains a possibility). The A-site interdiffusion could be rebalanced if approximately 6% of the Cr atoms in the first 4 u.c. of the LCO occupy an A site in place of a Sr atom. Theoretically, the additional p-type A^{2+} cations in the LCO could balance the n-type La^{3+} A-site doping in the STO. The oxidation state of the Cr that has diffused into the STO remains unclear, and the residual Ti^{3-4+} on the LCO side of the interface would still suggest a need for oxygen deficiency to balance the net charge of the system. While antisites are not directly observed near the interface in the HAADF-STEM data, it is not clear that a small number of Cr_A antisites would be distinguishable amid the gradual transition from Sr to La occupation at the A sites, as well as the potential intensity reduction that might arise in the case dechanneling near point defects. Low-angle annular dark-field (LAADF) STEM images, which have been shown to be very sensitive to point defects and strain,[41] do show an increased intensity at the interface, but this is typical of strained epitaxial heterojunctions and not conclusive.

Taking quantification attempts at face value would suggest a more significant fraction of Cr^{2+} at the interface than would be accounted for by antisites alone. Another possibility is that the Cr^{2+} forms by means of charge transfer from the STO, trapping the free electrons created near the interface by the effectively La-doped substrate. The charge offset induced by the effectively n-type STO side of the interface might align with unoccupied Cr t_{2g} states on the LCO side of the interface. Such a mechanism does not preclude the existence of a small fraction of Cr antisite defects or oxygen vacancies in the near-interface region of the LCO, which still seem likely given the aforementioned discussion. The same logic could apply, e.g., to B-site Mn and Fe near the interface of $LaBO_3$/STO, and $LaMnO_3$/STO at least has been found to be similarly insulating.[13]

The increased extent of interdiffusion with film thickness might offer an explanation for the critical thickness for the formation of a conductive interface in other polar/nonpolar perovskite interfaces,[42] particularly in the absence of B-site cations that can readily adopt a +2 charge state. The growth rate of LCO films is roughly constant and thus thicker films are held at growth temperatures (∼650 °C) for a longer time. This is consistent with thermally activated diffusion of cations, which is expected of cations in perovskites such as STO and LCO.[43] In particular given the possibility of site defects as discussed above, the diffusion rates of the different cations may not be equivalent. The balance of cations may well depend upon the total annealing time and temperature.

V. CONCLUSIONS

Cation intermixing and electronic states are examined in detail for the interface of LCO films grown on STO(001) by MBE using high-resolution HAADF-STEM, EDS, EFTEM, EELS, and HRRBS. All four cations are found to diffuse across the interface, with very low concentrations of La diffused deeply into the STO substrate. Incommensurate extents of interdiffusion are observed. However, it is found that there is extensive La diffusion into the STO, greater interdiffusion of A-site cations than for B-site cations, and a net charge that would not appear balanced if bulk cation valences were assumed. Yet the interfaces are thoroughly insulating. The near-edge structures of the Ti and Cr L edges indicate modification of the Ti and Cr valences towards Ti^{3+} and Cr^{2+} on the LCO side of the interface in a manner that should not resolve the apparent charge imbalance induced by cation interdiffusion. The presence of local oxygen vacancies cannot be ruled out, but the sub-1 at. % per u.c. oxygen deficiencies necessary to balance the net charge for the LCO/STO(001) films studied here would be difficult to definitively detect by any method. These results indicate that neither observations of cation imbalance nor charge reorganization alone at similar interfaces are necessarily sufficient to explain anomalous interfacial conductivity (or lack thereof). Additionally, the extent of interdiffusion increases with increasing film

thickness, suggesting that the cation gradation might be driven by strain reduction, or that cation interdiffusion is unavoidable at growth temperatures, or a combination of these effects. These results indicate that the formation of an abrupt interface in LCO/STO(001) may be limited to very thin films, a result that may extend to other similar perovskite oxide interfaces.

ACKNOWLEDGMENTS

Thanks are extended to T. Droubay for useful discussions. This work was supported by the US Department of Energy, Office of Basic Energy Sciences, Division of Materials Sciences and Engineering under Award No. 10122 (MBE and RBS), and the EMSL William Wiley Postdoctoral Fellowship program. The work was performed in the Environmental Molecular Sciences Laboratory, a national science user facility sponsored by the Department of Energy's Office of Biological and Environmental Research and located at Pacific Northwest National Laboratory. The authors also acknowledge support of the National Center for Electron Microscopy, Lawrence Berkeley National Laboratory, which is supported by the DOE BES under Contract No. DE-AC02-05CH11231.

[1] A. Ohtomo and H. Y. Hwang, Nature **427**, 423 (2004).
[2] M. Huijben, A. Brinkman, G. Koster, G. Rijnders, H. Hilgenkamp, and D. H. A. Blank, Adv. Mater. **21**, 1665 (2009).
[3] S. A. Chambers, Adv. Mater. **22**, 219 (2010).
[4] S. A. Chambers, M. H. Engelhard, V. Shutthanandan, Z. Zhu, T. Droubay, L. Qiao, P. Sushko, T. Feng, H. D. Lee, and T. Gustafsson, Surf. Sci. Rep. **65**, 317 (2010).
[5] S. A. Chambers, Surf. Sci. **605**, 1133 (2011).
[6] S. A. Pauli and P. R. Willmott, J. Phys.: Condens. Matter **20**, 264012 (2008).
[7] A. B. Shah, X. Zhai, B. Jiang, J. G. Wen, J. N. Eckstein, and J.-M. Zuo, Phys. Rev. B **77**, 115103 (2008).
[8] Ş. Smadici, P. Abbamonte, A. Bhattacharya, X. Zhai, B. Jiang, A Rusydi, J. N. Eckstein, S. D. Bader, and J.-M. Zuo, Phys. Rev. Lett. **99**, 196404 (2007).
[9] A. Bhattacharya, S. J. May, S. G. E. te Velthuis, M. Warusawithana, X. Zhai, B. Jiang, J.-M. Zuo, M. R. Fitzsimmons, S. D. Bader, and J. N. Eckstein, Phys. Rev. Lett. **100**, 257203 (2008).
[10] J. Garcia-Barriocanal, J. C. Cezar, F. Y. Bruno, P. Thakur, N. B. Brookes, C. Utfeld, A. Rivera-Calzada, S. R. Giblin, J. W. Taylor, J. A. Duffy, S. B. Dugdale, T. Nakamura, K. Kodama, C. Leon, S. Okamoto, and J. Santamaria, Nat. Commun. **1**, 82 (2010).
[11] A. B. Shah, Q. M. Ramasse, X. Zhai, J. G. Wen, S. J. May, I. Petrov, A. Bhattacharya, P. Abbamonte, J. N. Eckstein, and J.-M. Zuo, Adv. Mater. **22**, 1156 (2010).
[12] P. Moetakef, T. A. Cain, D. G. Ouellette, J. Y. Zhang, D. O. Klenov, A. Janotti, C. G. Van de Walle, S. Rajan, S. J. Allen, and S. Stemmer, Appl. Phys. Lett. **99**, 232116 (2011).
[13] P. Perna, D. Maccariello, M. Radovic, U. Scotti di Uccio, I. Pallecchi, M. Codda, D. Marre, C. Cantoni, J. Gazquez, and M. Varela, Appl. Phys. Lett. **97**, 152111 (2010).
[14] C. He, T. D. Sanders, M. T. Gray, F. J. Wong, V. V. Mehta, and Y. Suzuki, Phys. Rev. B **86**, 081401(R) (2012).
[15] Y. Hotta, T. Susaki, and H. Y. Hwang, Phys. Rev. Lett. **99**, 236805 (2007).
[16] M. Luysberg, M. Heidelmann, L. Houben, M. Boese, T. Heeg, J. Schubert, and M. Roeckerath, Acta Mater. **57**, 3192 (2009).
[17] A. Kalabukhov, Y. A. Boikov, I. T. Serenkov, V. I. Sakharov, J. Börjesson, N. Ljustina, E. Olsson, D. Winkler, and T. Claeson, EPL **93**, 37001 (2011).
[18] S. A. Chambers, L. Qiao, T. C. Droubay, T. C. Kaspar, B. W. Arey, and P. V. Sushko, Phys. Rev. Lett. **107**, 206802 (2011).
[19] D. G. Schlom and J. Mannhart, Nat. Mater. **10**, 168 (2011).
[20] J. Mannhart and D. G. Schlom, Science **327**, 1607 (2010).
[21] N. Nakagawa, H. Y. Hwang, and D. A. Muller, Nat. Mater. **5**, 204 (2006).
[22] J. L. Maurice, I. Devos, M. J. Casanove, C. Carrétéro, G. Gachet, G. Herranz, D. G. Crété, D. Imhoff, A. Barthélémy, M. Bibes, K. Bouzehouane, C. Deranlot, S. Fusil, É. Jacquet, B. Domengès, and D. Ballutaud, Mater. Sci. Eng., B **144**, 1 (2007).
[23] J. L. Maurice, G. Herranz, C. Colliex, I. Devos, C. Carrétéro, A. Barthélémy, K. Bouzehouane, S. Fusil, D. Imhoff, É. Jacquet, F. Jomard, D. Ballutaud, and M. Basletic, EPL **82**, 17003 (2008).
[24] V. Vonk, J. Huijben, D. Kukuruznyak, A. Stierle, H. Hilgenkamp, A. Brinkman, and S. Harkema, Phys. Rev. B **85**, 045401 (2012).
[25] P. R. Willmott, S. A. Pauli, R. Herger, C. M. Schlepütz, D. Martoccia, B. D. Patterson, B. Delley, R. Clarke, D. Kumah, C. Cionca, and Y. Yacoby, Phys. Rev. Lett. **99**, 155502 (2007).
[26] Y. Segal, J. H. Ngai, J. W. Reiner, F. J. Walker, and C. H. Ahn, Phys. Rev. B **80**, 241107 (2009).
[27] M. Takizawa, S. Tsuda, T. Susaki, H. Y. Hwang, and A. Fujimori, Phys. Rev. B **84**, 245124 (2011).
[28] L. Qiao, T. C. Droubay, M. E. Bowden, V. Shutthanandan, T. C. Kaspar, and S. A. Chambers, Appl. Phys. Lett. **99**, (2011).
[29] L. Giannuzzi, J. Drown, S. Brown, R. Irwin, and F. Stevie, Microsc. Res. Tech. **41**, 285 (1998).
[30] P. Cueva, R. Hovden, J. A. Mundy, H. L. Xin, and D. A. Muller, Microsc. Microanal. **18**, 970 (2012).
[31] M. Mayer, in *The Fifteenth International Conference on the Application of Accelerators in Research and Industry* (AIP, New York, 1999), pp. 541–544.
[32] B. Kabius, P. Hartel, M. Haider, H. Muller, S. Uhlemann, U. Loebau, J. Zach, and H. Rose, J. Electron Microsc. **58**, 147 (2009).
[33] R. F. Egerton, *Electron Energy-Loss Spectroscopy in the Electron Microscope* (Springer Science + Business Media, New York, 2011).
[34] R. Moos and K. H. Hardtl, J. Am. Ceram. Soc. **80**, 2549 (2005).
[35] S. R. Sutton, K. W. Jones, B. Gordon, M. L. Rivers, S. Bajt, and J. V. Smith, Geochim. Cosmochim. Acta **57**, 461 (1993).
[36] A. Ohtomo, D. A. Muller, J. L. Grazul, and H. Y. Hwang, Appl. Phys. Lett. **80**, 3922 (2002).
[37] T. L. Daulton and B. J. Little, Ultramicroscopy **106**, 561 (2006).

[38]D. H. Pearson, C. C. Ahn, and B. Fultz, Phys. Rev. B **47**, 8471 (1993).

[39]See Supplemental Material at http://link.aps.org/supplemental/10.1103/PhysRevB.88.155325 for cation valence state quantification from ELNES analysis.

[40]L. Qiao, K. H. L. Zhang, M. E. Bowden, T. Varga, V. Shutthanandan, R. Colby, Y. Du, B. Kabius, P. V. Sushko, M. D. Biegalski, and S. A. Chambers, Adv. Funct. Mater. **23**, 2953 (2013).

[41]D. Muller, N. Nakagawa, A. Ohtomo, J. Grazul, and H. Hwang, Nature **430**, 657 (2004).

[42]S. Thiel, Science **313**, 1942 (2006).

[43]R. Riedel, I. Chen, *Ceramics Science and Technology*, (Wiley-VCH, Weinheim, 2008), Vol. 1.